Altering the Binuclear Manganese Cluster of Arginase Diminishes Thermostability and Catalytic Function†

Laura R. Scolnick,‡ Zoltan F. Kanyo,‡,§ R. Christopher Cavalli,|| David E. Ash,*,|| and David W. Christianson*,‡

Department of Chemistry, University of Pennsylvania, 231 South 34th Street, Philadelphia, Pennsylvania 19104-6323, and Department of Biochemistry, Temple University School of Medicine, 3420 North Broad Street, Philadelphia, Pennsylvania 19140

Received April 7, 1997; Revised Manuscript Received June 30, 1997⊗

ABSTRACT: Arginase is a thermostable (T_m = 75 °C) binuclear manganese metalloenzyme which hydrolyzes L-arginine to form L-ornithine and urea. The three-dimensional structures of native metal-depleted arginase, metal-loaded H101N arginase, and metal-depleted H101N arginase have been determined by X-ray crystallographic methods to probe the roles of the manganese ion in site A (Mn^{2+}_A) and its ligand H101 in catalysis and thermostability. We correlate these structures with thermal stability and catalytic activity measurements reported here and elsewhere [Cavalli, R. C., Burke, C. J., Kawamoto, S., Soprano, D. R., and Ash, D. E. (1994) *Biochemistry 33,* 10652−10657]. We conclude that the substitution of a wild-type histidine ligand to Mn^{2+}_A compromises metal binding, which in turn compromises protein thermostability and catalytic function. Therefore, a fully occupied binuclear manganese metal cluster is required for optimal catalysis and thermostability.

Arginase is a binuclear manganese metalloenzyme that catalyzes the hydrolysis of L-arginine to form L-ornithine and urea (L-arginine amidinohydrolase, EC 3.5.3.1). This reaction comprises the final cytosolic step of the urea cycle, which provides the principal route for the disposal of nitrogenous waste from protein catabolism. Although arginase activity is most abundant in mammalian liver where the urea cycle is most active (Herzfeld & Raper, 1976), arginase activity is also found in nonhepatic cells and tissues such as the red blood cell (Kedra-Luboinska et al., 1988), the lactating mammary gland (Yip & Knox, 1972), the kidney (Herzfeld & Raper, 1976), the myometrium (Weiner et al., 1996), and the macrophage (Currie, 1978). The function of arginase in nonhepatic locations is to modulate arginine and ornithine concentrations for biosynthesis. For example, L-ornithine is a biosynthetic precursor of L-proline (Yip & Knox, 1972) and the polyamines spermine and spermidine (Tabor & Tabor, 1984). In other tissues, L-arginine is a biosynthetic precursor of nitric oxide (NO). In the macrophage, arginase is reciprocally regulated with NO synthase in order to modulate NO-dependent cytotoxicity (Stuehr et al., 1991; Daghigh et al., 1994; Boutard et al., 1995; Corraliza et al., 1995; Modolell et al., 1995; Wang et al., 1995; Southan & Szabo, 1996; Morris et al., 1997).

The 2.1-Å resolution crystal structure of trimeric rat liver arginase reveals that the binuclear manganese cluster resides at the base of a 15 Å deep active site cleft in each monomer (Figure 1; Kanyo et al., 1996). Analysis of the native enzyme structure suggests that arginine hydrolysis is achieved

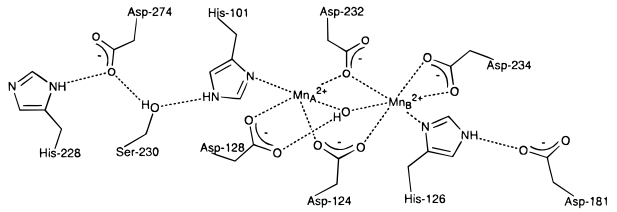

FIGURE 1: Scheme of the binuclear manganese cluster of native arginase (Kanyo et al., 1996). Histidine metal ligands are nested within hydrogen bond networks as indicated.

by a metal-activated solvent molecule which symmetrically bridges the two Mn^{2+} ions. The metal ion that is more deeply situated in the active-site cleft (designated Mn^{2+}_A) is coordinated by H101 (Nδ), D124 (Oδ1), D128 (Oδ1), D232 (Oδ1), and the bridging solvent molecule with square pyramidal geometry. The second metal ion (designated Mn^{2+}_B) is coordinated by H126 (Nδ), D124 (Oδ2), D234 (Oδ1), D232 (bidentate Oδ1 and Oδ2), and the bridging solvent molecule in distorted octahedral fashion. The Mn^{2+}_A−Mn^{2+}_B separation is 3.3 Å. Except for D128, all metal ligands make hydrogen bond interactions with the protein scaffold which contribute to the stability of the metal binding site. In general, hydrogen bond interactions with histidine metal ligands are known to fine-tune the stability and reactivity of protein−metal sites (Christianson & Alexander, 1989). In arginase, H101 donates a hydrogen bond to S230, which in turn donates a hydrogen bond to D274; H126 donates a hydrogen bond to D181 (Figure 1). Notably, histidine metal ligands are conserved among all 15 arginase isozymes identified from mammalian, bacterial, and yeast sources (Morris et al., 1997).

In order to probe the importance of histidine metal ligands for the stability and catalytic activity of the binuclear manganese cluster, we have determined the X-ray crystal structures of native arginase and recombinant H101N[1] arginase in the metal-loaded and metal-depleted states.[2] Specifically, we have determined the structures of metal-

† Supported by NIH Grants GM49758 to D.W.C. and DK44841 to D.E.A. L.R.S. was supported in part by Cell and Molecular Biology Training Grant GM07229.

* Authors to whom correspondence should be addressed.

‡ University of Pennsylvania.

§ Current address: Department of Neurology, University of California, 515 Parnassus Ave., San Francisco, California 94143.

|| Temple University School of Medicine.

⊗ Abstract published in *Advance ACS Abstracts,* August 15, 1997.

S0006-2960(97)00800-3 CCC: $14.00

Table 1: Data Collection and Refinement Statistics

	metal-depleted native arginase (pH 8.5)	metal-loaded H101N arginase (pH 9.0)	metal-depleted H101N arginase (pH 9.0)	metal-depleted H101N arginase (pH 8.5)
unit cell parameters (Å)	$a = b = 88.5$, $c = 106.0$	$a = b = 89.0$, $c = 115.4$	$a = b = 89.1$, $c = 115.1$	$a = b = 88.9$, $c = 105.1$
no. of crystals	1	1	1	1
no. of measured reflections	17377	65410	24335	37872
no. of unique reflections	14894	26381	18429	23414
maximum resolution (Å)	3.0	2.5	2.9	2.7
completeness of data (%)	80.2	74.0	81.4	91.8
R_{sym}[a]	0.064	0.105	0.094	0.091
no. of water molecules in final cycle of refinement	24	20	15	27
no. of reflections used in refinement ($>2\sigma$)	14349	25411	17477	22421
R_{free}[b]	0.299	0.282	0.246	0.270
R_{cryst}[c]	0.197	0.194	0.176	0.175
rmsd, bonds (Å)	0.010	0.013	0.008	0.012
rmsd, angles (deg)	1.4	1.7	1.4	1.7
rmsd, dihedrals (deg)	23.7	24.3	23.8	24.4
rmsd, impropers (deg)	1.4	1.6	1.3	1.6

[a] $R_{sym} = \sum|I_i - \langle I_i\rangle|/\sum\langle I_i\rangle$; I_i = intensity measured for reflection i; $\langle I_i\rangle$ = average intensity for reflection i calculated from replicate data. [b] $R_{free} = \sum||F_o| - |F_c||/\sum|F_o|$ calculated for reflections belonging to a test set of 10% of the unique reflections omitted from refinement; $|F_o|$ and $|F_c|$ are the observed and scaled calculated structure factor amplitudes, respectively. [c] $R_{cryst} = \sum||F_o| - |F_c||/\sum|F_o|$; $|F_o|$ and $|F_c|$ are the observed and scaled calculated structure factor amplitudes, respectively.

depleted native arginase, metal-loaded H101N arginase, and metal-depleted H101N arginase. We correlate these structures with thermostability and catalytic activity measurements reported here and by Cavalli and colleagues (1994). Importantly, an intact binuclear manganese cluster is required for optimal thermostability and maximal catalytic activity: dialysis of Mn^{2+}_A out of the native enzyme active site compromises catalysis and thermostability. Likewise, the substitution of a wild-type histidine ligand to Mn^{2+}_A compromises metal binding, which in turn compromises catalysis and thermostability. Finally, differences between the crystal structures of metal-depleted H101N arginase determined at pH 8.5 and pH 9.0 reflect the molecular basis of a characteristic pH-dependent change in crystal morphology, namely, a 10 Å increase in the length of the *c*-axis at higher pH values (Kanyo et al., 1992).

MATERIALS AND METHODS

Circular Dichroism Spectroscopy. Spectra were recorded on an Aviv 62DS spectropolarimeter interfaced with an IBM PC. A circulating water bath maintained the temperature of the sample cell at 25 °C. Protein samples were diluted to 1−2.5 μM trimer in either 5 mM Tris-HCl, 100 μM $MnCl_2$, pH 7.5, or 5 mM Tris-HCl, 1 mM EDTA, pH 7.5. Samples in 0.1 cm quartz cells were equilibrated for 5 min at room temperature before each spectrum was recorded. The temperature was increased in 2 °C intervals with a 2 min equilibration time at each temperature. Thermal transitions were monitored by following the change in ellipticity at 222 nm ($[\theta_{222}]$). The fraction of unfolded protein at each temperature was determined by calculating the ratio $[\theta_{222}]/[\theta_{222}]_d$, where $[\theta_{222}]_d$ is the molar ellipticity for the completely denatured enzyme.

Crystallography. The crystallization of rat liver arginase has been reported previously (Kanyo, et al., 1992). Crystals of metal-depleted native arginase[2] were prepared by gradually transferring crystals to a buffer solution containing 50 mM bicine (pH 8.5 at room temperature), 40% PEG 8000, 20 mM dipicolinic acid (DPA), and 20 mM disodium ethylenediaminetetraacetate (EDTA) for 1 week at 4 °C.

Recombinant H101N arginase expressed in *E. coli* and purified as described (Cavalli et al., 1994) was crystallized by the sitting drop method at 4 °C. Typically, a 5-μL drop containing 6−8 mg/mL enzyme and 50 mM bicine (pH 9.0 at room temperature) was added to a 5-μL drop containing 50 mM bicine (pH 9.0 at room temperature), 14−16% PEG 8000, 0.05% sodium azide, and 1 mM $MnCl_2$ in the crystallization well. The drop was equilibrated against 1 mL of precipitant buffer in the well reservoir. Crystals of H101N arginase at pH 8.5 were nearly isomorphous with those of native enzyme (Kanyo et al., 1992) and belonged to space group $P3_2$ with unit cell parameters of $a = 89.0$ Å, $b = 89.0$ Å, and $c = 105.1$ Å. At pH 9.0, crystals of H101N arginase exhibited a characteristic pH-dependent increase in the *c*-axis length (Kanyo et al., 1992) with unit cell parameters of $a = 89.0$ Å, $b = 89.0$ Å, and $c = 115.0$ Å. Crystals of metal-depleted H101N arginase[2] were prepared by gradually transferring crystals to a buffer solution containing 50 mM bicine (pH 9.0 at room temperature), 20% PEG 8000, 15 mM DPA, and 15 mM EDTA for 1 week at 4 °C.

Crystals were mounted in 0.5 or 0.7 mm glass capillaries with a small portion of mother liquor and sealed with wax. X-ray diffraction data were collected using an R-AXIS IIc image plate detector mounted on an RU-200HB rotating anode generator with double focusing mirrors operating at 50 kV/100 mA. Data were collected in successive 11−15 min 2° oscillations about ϕ for a total scan range of 75°; the crystal-to-detector distance was set at 115 mm, and the swing angle 2θ was set at 0°. The crystal orientation was established with REFIX (Kabsch, 1993), and data were reduced using MOSFLM (Nyborg & Wonacott, 1977). Data reduction was completed with CCP4 (Collaborative Computational Project, 1994); relevant statistics are recorded in Table 1.

[1] Abbreviations: H101N, histidine-101→asparagine; EDTA, disodium ethylenediaminetetraacetate; DPA, dipicolinic acid.

[2] Throughout this paper, the terms "metal-loaded" and "metal-depleted" specifically refer to arginase samples containing 2 Mn^{2+}/active site and 1 Mn^{2+}/active site, respectively.

Initial phases for each electron density map were obtained by molecular replacement using AMoRe (Navaza, 1994) as implemented in CCP4. The atomic coordinates of the refined native arginase structure (Kanyo et al., 1996) were used as a search probe in rotation and translation function calculations, which yielded unique and unambiguous solutions for each structure (Scolnick, 1997). The starting coordinate set for the refinement of each variant was that of the native arginase monomer with the H101 side chain and all water molecules deleted from the model. Each structure was refined by simulated annealing with energy minimization as implemented in X-PLOR (Brünger et al., 1987). Individual *B*-factors were refined, and a bulk solvent correction was applied. In the final stages of refinement, the quality of the model was improved by gradually releasing the noncrystallographic symmetry constraints into appropriately-weighted restraints as judged by R_{free}. The graphics software CHAIN (Sack, 1988), installed on a Silicon Graphics Indigo workstation, was utilized for all map-fitting procedures. Electron density peaks in the solvent region were interpreted as water molecules if their peak heights $>2.5\sigma$, if they were found within hydrogen bonding distance of appropriate protein atoms, and if they refined with thermal *B*-factors ≤ 50 Å^2.

For each variant, refinement converged smoothly to final crystallographic *R* factors within the range 0.175−0.197; all pertinent refinement statistics are recorded in Table 1. For each structure, the rms error in atomic positions was estimated to be ca. 0.12−0.34 Å using SIGMA-A (Read, 1986). Atomic coordinates have been deposited in the Brookhaven Protein Data Bank (Bernstein et al., 1977) with accession codes 2RLA (metal-depleted native arginase at pH 8.5), 3RLA (metal-loaded H101N arginase at pH 9.0), 4RLA (metal-depleted H101N arginase, at pH 9.0), and 5RLA (metal-depleted H101N arginase at pH 8.5).

RESULTS

CD Spectroscopy. The midpoints of the thermal transitions, T_m, for wild-type and H101N arginases measured in the presence of 100 μM $MnCl_2$, (i.e., ensuring an intact binuclear manganese cluster) are 75 ± 2 and 61 ± 2 °C, respectively (Figure 2a). The stability of metal-loaded wild-type arginase is comparable to that reported by Cavalli and colleagues (1994); however, the T_m value of metal-loaded H101N arginase reported here is about 7 °C lower than that reported by Cavalli and colleagues (1994). The T_m values for wild-type and H101N arginases measured in the presence of 1 mM EDTA are 60 ± 2 °C and 52 ± 2 °C, respectively. These results demonstrate that compromising the binuclear manganese cluster in any way—either by partial metal depletion or by ligand substitution—compromises the exceptional thermostability of the enzyme (Figure 2b). Therefore, an intact binuclear manganese cluster is important for the optimal stabilization of the folded state due to the strong ligand−metal coordination interactions which effectively cross-link amino acid residues distant in sequence.

Crystallography. Despite local structural differences in the vicinity of the metal binding site(s), the overall structures of metal-depleted native arginase, metal-loaded H101N arginase, and metal-depleted H101N arginase are quite similar.[2] the rms deviation of Cα atoms between each arginase structure and that of metal-loaded native arginase (Kanyo et al., 1996) are in the range 0.28−0.34 Å. In the remainder of this section, we outline the features responsible

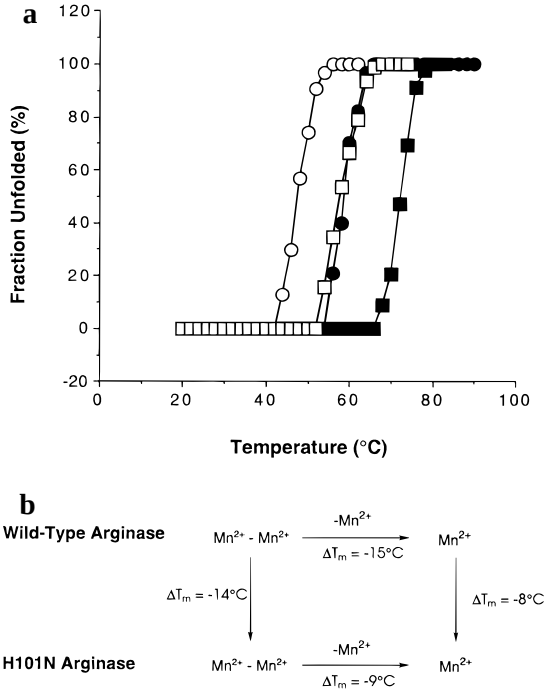

FIGURE 2: (a) Temperature-dependent unfolding of wild-type and H101N arginases in metal-loaded and metal-depleted states as monitored by changes in ellipticity at 222 nm [θ_{222}]: (■) metal-loaded wild-type arginase; (□) metal-depleted wild-type arginase; (●) metal-loaded H101N arginase; (○) metal-depleted H101N arginase. (b) Comparison of T_m values indicates that altering wild-type $Mn^{2+}{}_A$ ligand H101 compromises thermostability of arginase; $Mn^{2+}{}_A$ depletion also destabilizes the enzyme.

for diminished thermostability and compromised catalytic activity in arginase structures containing a compromised binuclear manganese cluster.

Metal-Depleted Native Arginase. The difference electron density map of Figure 3 reveals that only $Mn^{2+}{}_B$ remains bound in the active site upon soaking native arginase crystals in a buffer solution containing 20 mM EDTA and 20 mM DPA for 1 week. Therefore, we conclude that $Mn^{2+}{}_A$ is the more weakly-bound manganese ion of the binuclear manganese cluster implicated by the studies of Hirsch-Kolb and colleagues (1971). Although the 3.0 Å resolution of this structure is relatively modest, the superposition of this structure with metal-loaded arginase shown in Figure 4 reveals that no significant disordering of $Mn^{2+}{}_A$ ligands results from metal dissociation. Metal ligands appear to be preorganized for metal complexation by hydrogen bond interactions with neighboring residues. For example, $Mn^{2+}{}_A$ ligand H101 donates a hydrogen bond to S230, which in turn donates a hydrogen bond to D274 (Figure 1). Hydrogen bond interactions with histidine metal ligands enhance protein−metal affinity and fine-tune the reactivity of metal-bound solvent (Christianson & Alexander, 1989; Kiefer et al., 1995; Lesburg & Christianson, 1995).

Aspartate metal ligands also accept hydrogen bonds from neighboring donor residues. Although these particular interactions must weaken the electrostatic interaction between the carboxylate group and a coordinated metal ion, these interactions nonetheless preorganize the carboxylate groups with optimal metal complexation geometry and therefore minimize the conformational entropy cost otherwise associated with metal complexation. For example, the carboxylate oxygens of D124 accept *anti*-oriented hydrogen bonds from

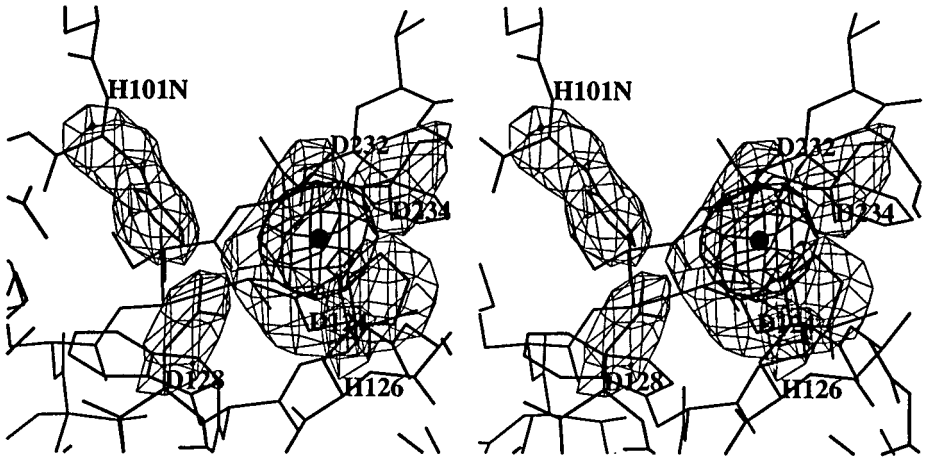

FIGURE 3: Omit maps of the metal-depleted native arginase calculated with Fourier coefficients $|F_o| - |F_c|$ and phases caculated from the final model less the atoms of metal ligands (contoured at 2σ) or metal ion $Mn^{2+}{}_B$ (contoured at 3σ). Metal ligands are indicated, and $Mn^{2+}{}_B$ appears as a sphere. Note the well-defined electron density for all ligands in the empty $Mn^{2+}{}_A$ site.

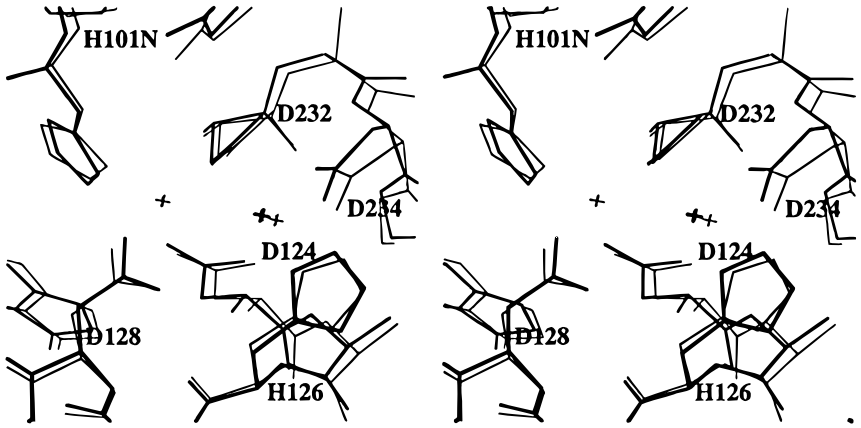

FIGURE 4: Least-squares superposition of metal-depleted (thick bonds) and metal-loaded (thin bonds) native arginases. Metal ligands are labeled with residue name and sequence number, and metal ion locations are indicated by stars. The protein appears to be preorganized for optimal metal binding conformation in metal site A.

the side chain NH group of W122 and the backbone NH group of A125, and the Oδ2 atom of D232 (the "dangling" oxygen of the bridging monodentate ligand) accepts an *anti*-oriented hydrogen bond from the backbone NH group of D234. These interactions are maintained despite metal dissociation from site A.

Both the position and the coordination geometry of $Mn^{2+}{}_B$ remain relatively unchanged compared with native metal-loaded arginase, so we conclude that metal dissociation from site A does not significantly perturb the metal ion in site B. Given the moderate resolution (3 Å) of this structure, extensive solvent structure is not visible in the electron density map. We cannot see a solvent molecule bound to $Mn^{2+}{}_B$ which would correspond to the bridging solvent molecule in the intact binuclear manganese cluster of the native enzyme (Kanyo et al., 1996).

Interpretation of these structures in light of the significant loss of thermostability measured for recombinant wild-type arginase suggests that $Mn^{2+}{}_A$ binding makes a significant contribution to the exceptional thermostability of native metal-loaded arginase. Each manganese ion makes strong coordination interactions which effectively cross-link amino acid residues distant in sequence, and these interactions stabilize the folded state of the protein. The binuclear manganese cluster is thus a critical structural component of the protein, and perturbation of this cluster by metal dissociation compromises the stability of the metal binding site as well as the overall structure.

Metal-Loaded H101N Arginase. The difference electron density map in Figure 5 reveals a binuclear manganese cluster in which metal binding to site A is partially compromised despite the equilibration of these crystals in buffer solutions containing 1 mM $MnCl_2$. Crystallographic refinement results suggest that $Mn^{2+}{}_A$ is bound with approximately 60% occupancy and $Mn^{2+}{}_B$ is bound with 100% occupancy. Surprisingly, there is no significant electron density for the engineered side chain of N101 beyond the Cβ atom, an indication that this potential metal ligand is disordered despite the significant occupancy of manganese in site A. Modeling of the N101 conformation in the refined structure of metal-loaded H101N arginase suggests that this side chain can adopt three different yet energetically-favorable conformations without contacting neighboring residues; two of these conformations would allow N101 to make reasonable metal coordination interactions, but none of these conformations would allow N101 to donate a hydrogen bond to S230. The loss of this hydrogen bond interaction, which orients wild-type H101 for optimal $Mn^{2+}{}_A$ coordination (e.g., see Figure 1), may contribute to the observed disorder of the N101 side chain. We conclude that the substitution of the single histidine ligand to $Mn^{2+}{}_A$ with asparagine compromises the stability of the binuclear manganese cluster, as reflected by

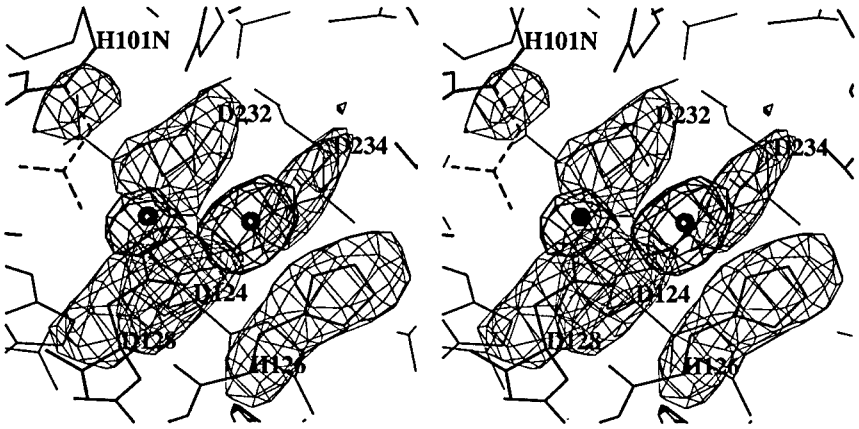

FIGURE 5: Omit maps of metal-loaded H101N arginase calculated with $|F_o| - |F_c|$ and phases calculated from the final model less the atoms of metal ligands (contoured at 7.5σ) or metal ion Mn^{2+}_B (contoured at 10σ). Metal ligands are indicated, and the two Mn^{2+} ions appear as spheres. Note that electron density for the variant N101 side chain does not extend beyond Cβ, which implies conformational disorder. The N101 side chain is therefore modeled in a conformation similar to that of the wild-type H101 side chain (dashed lines).

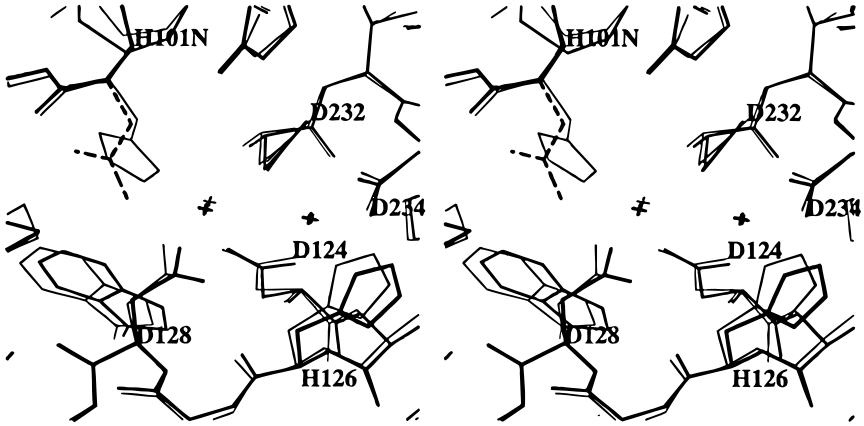

FIGURE 6: Least-squares superposition of metal-loaded H101N arginase (thick bonds) and metal-loaded native arginase (thin bonds). Metal ligands are indicated, and Mn^{2+} ion positions are indicated by stars.

partial-occupancy metal binding in site A of this variant. Other than the lack of a well-ordered coordination interaction with N101, no other significant changes are observed for the positions and coordination geometries of Mn^{2+}_A ligands (Figure 6). The refined Mn^{2+}_A−Mn^{2+}_B separation is 3.3 Å and is unchanged from the native enzyme (Kanyo et al., 1996).

Both the position and the coordination geometry of Mn^{2+}_B remain relatively unchanged in comparison with native metal-loaded arginase, so we conclude that the H101N substitution in site A does not perturb the metal ion in site B (Figure 6). Given the 2.5 Å resolution of this crystal structure, some solvent molecules are observed in the electron density map and are included in the final model as designated in Table 1. However, the bridging solvent molecule in the binuclear manganese cluster is not visible at this resolution.

Thermostability measurements conducted in the presence of 100 μM $MnCl_2$ (conditions that will ensure the binding of Mn^{2+} in site A) demonstrate that despite the preservation of the binuclear manganese cluster under these conditions, H101N arginase exhibits significantly compromised thermostability. Indeed, compromised thermostability in this variant rivals that observed for the metal-depleted native enzyme (Figure 2). Therefore, we conclude that H101 effectively cross-links the protein structure through its coordination interaction with Mn^{2+}_A, and the loss of this stabilizing interaction in the binuclear manganese cluster is responsible for compromised thermostability.

Metal-Depleted H101N Arginase. The difference electron density map of Figure 7 reveals that only Mn^{2+}_B remains bound in the active site upon soaking of H101N arginase crystals in buffer solutions containing 15 mM EDTA and 15 mM DPA for 1 week. This result is consistent with the metal dissociation behavior observed in crystals of the native enzyme, namely, that Mn^{2+}_A is the more weakly-bound manganese ion identified by Hirsch-Kolb and colleagues (1971). The substitution of the wild-type histidine ligand to Mn^{2+}_A must further weaken metal affinity in site A. The superposition of this structure with that of metal-loaded H101N arginase (Figure 8) reveals no significant structural differences in Mn^{2+}_A ligands resulting from metal dissociation. However, just as observed in metal-loaded H101N arginase, significant electron density for the side chain of N101 is absent beyond the Cβ atom (Figure 7). If a metal coordination interaction is not sufficient to fix this side chain in one principal conformation, then it is not surprising that this side chain remains disordered upon metal dissociation. Possibly, the dramatic loss of catalytic activity for metal-depleted H101N arginase compared with metal-depleted native arginase (Cavalli et al., 1994) is due to unfavorable interactions between the disordered N101 side chain and D128, which may hydrogen bond to metal-bound solvent and serve as a proton shuttle residue in catalysis (Kanyo et al., 1996).

Both the position and the coordination geometry of Mn^{2+}_B remain relatively unchanged compared with metal-loaded

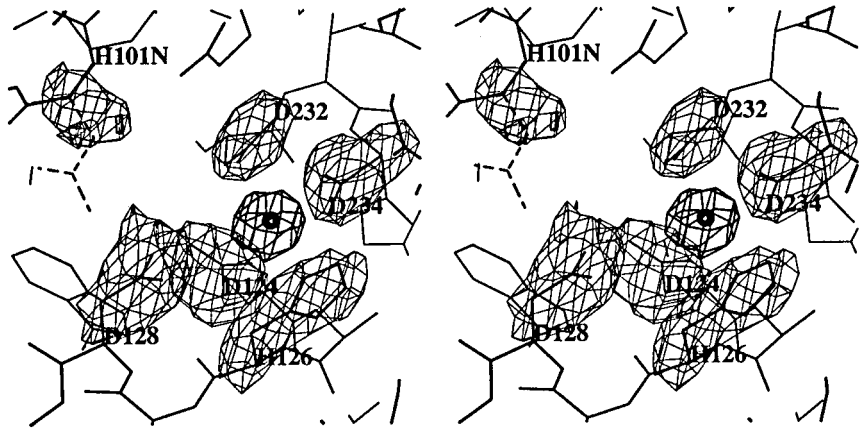

FIGURE 7: Omit maps of metal-depleted H101N arginase calculated with $|F_o| - |F_c|$ and phases caculated from the final model less the atoms of metal ligands (contoured at 7.5σ) or metal ion $Mn^{2+}{}_B$ (contoured at 10σ). Metal ligands are indicated, and the metal ion appears as a sphere. Note that electron density for the variant N101 side chain does not extend beyond Cβ, which implies conformational disorder. The N101 side chain is therefore modeled in a conformation similar to that of the wild-type H101 side chain (dashed lines).

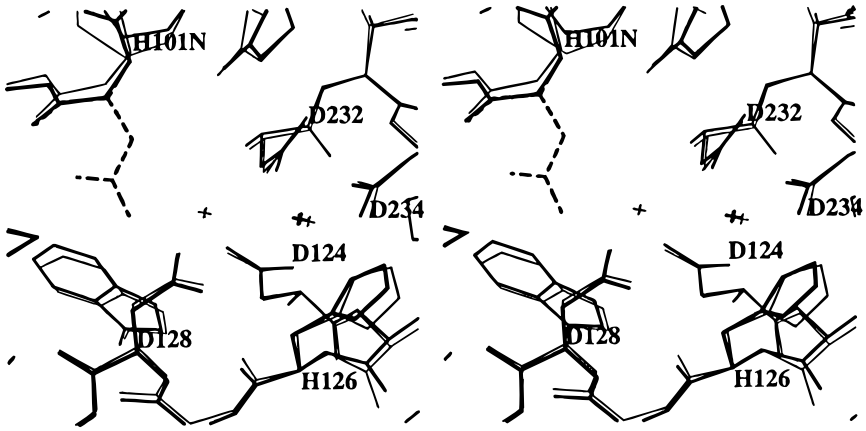

FIGURE 8: Least-squares superposition of metal-loaded (thick bonds) and metal-depleted H101N arginases (thin bonds). Apart from the disorder of the N101 side chain (dashed line), the metalloenzyme variant appears to be preorganized for Mn^{2+} binding in site A.

native or H101N arginases, so we conclude that metal dissociation from site A does not perturb the metal ion in site B, regardless of the identity of residue 101. Due to the moderate resolution of the crystal structure, we cannot see a solvent molecule bound to $Mn^{2+}{}_B$ which would correspond to the bridging solvent molecule in the intact binuclear manganese cluster.

The structure of metal-depleted H101N arginase was determined at pH 8.5 and pH 9.0. Although the pH optimum of catalytic activity is in the range 9.0−9.5 (Roholt & Greenberg, 1956; Cavalli et al., 1994), no significant pH-dependent structural differences are observed in the active site of this metal-depleted arginase variant. In the absence of any significant pH-dependent structural changes, we propose that increased activity at higher pH values for metal-loaded and metal-depleted arginases arises from a higher concentration of the catalytic nucleophile, metal-bound hydroxide, at alkaline pH values.

Interestingly, arginase crystals undergo a significant morphology change in the pH range 8.5−9.0: the *c*-axis elongates by approximately 10% as the pH is increased from 8.5 to 9.0 (Kanyo et al., 1992). Comparable nonisomorphism accompanied the preparation of heavy atom derivatives and was a significant hindrance in the phasing of the initial electron density map (Kanyo et al., 1996). As the pH 8.5 and pH 9.0 structures of metal-depleted H101N arginase are compared, no significant differences in tertiary or quaternary structure are observed. However, the orientation of the trimer in the unit cell appears to tilt by an additional 2−3° relative to the *c*-axis at pH 9.0. Comparison of the interlattice contacts at pH 8.5 and pH 9.0 suggests that a single lysine residue, K33, may possibly trigger changes in interlattice contacts at higher pH values. The superposition of metal-depleted H101N arginase structures at pH 8.5 and pH 9.0 shows that K33 makes no significant interactions at pH 8.5, but at pH 9.0 it is buried in a small pocket on an adjacent trimer and makes possible hydrogen bonds with Q88, S271, and T92. Possibly, K33 is not stable in this buried location with a positively-charged side chain, regardless of the hydrogen bond opportunities. Since the pH-dependence of the crystal morphology change correlates most closely with the pK_a of a lysine side chain, and since K33 is the only lysine residue making significant interlattice contacts, it is possible that K33 is largely responsible for the pH-dependent change in the *c*-axis length.

DISCUSSION

Implications for Catalysis. Histidine is a common metal ligand in the active sites of metalloenzymes. In rat liver arginase, Nδ of H101 coordinates to $Mn^{2+}{}_A$ with a metal−ligand separation of 2.2 Å, and Nϵ donates a hydrogen bond to the γ-OH group of S230 (N−O separation = 2.8 Å). The disorder of N101 in metal-loaded and metal-depleted H101N arginase suggests that an asparagine→metal coordination interaction at position 101 is not favorable due to the weaker metal coordination behavior of the asparagine carbonyl in

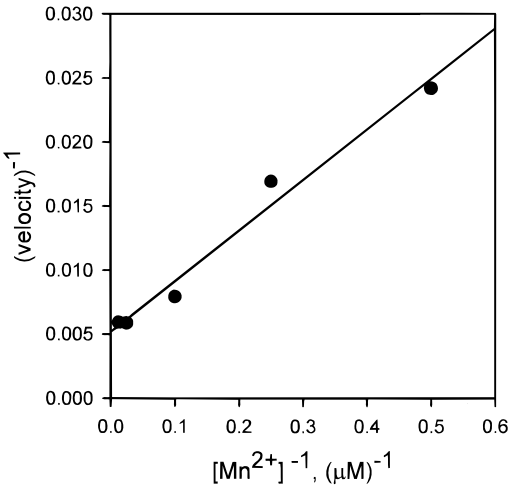

FIGURE 9: Double-reciprocal plot of the Mn^{2+} activation of metal-depleted H101N arginase. Assays were performed as described (Cavalli et al., 1994) and contained 100 mM bicine and 20 mM arginine at pH 9. Velocities are in arbitrary units.

comparison with the histidine imidazole nitrogen of the native enzyme. Additionally, the loss of a stabilizing hydrogen bond between N101 and S230, which potentially could have preoriented N101 for metal coordination, must contribute to the destabilization of metal binding in site A. The k_{cat} of metal-loaded H101N arginase is 118 s^{-1} (i.e., 47% of that measured for metal-loaded wild-type arginase), and the k_{cat} of metal-depleted H101N arginase is 0.51 s^{-1} when measured in the presence of 10 mM EDTA (i.e., 0.17% of that measured for metal-loaded wild-type arginase; Cavalli et al., 1994). Since no major global structural changes accompany the H101N substitution, we propose that the 2-fold loss of catalytic activity measured for metal-loaded H101N arginase is due to the slight structural perturbation of the binuclear manganese cluster resulting from the H101N substitution and the disorder of the N101 side chain. The massive loss of catalytic activity measured for metal-depleted H101N arginase shows that an intact binuclear manganese cluster is necessary for the optimal catalytic function of this variant: two metal ions can polarize a nucleophilic solvent molecule better than a single metal ion. We hypothesize that unfavorable interactions between the disordered N101 side chain and the catalytic nucleophile may also contribute to this activity loss.

That metal-depleted H101N arginase can be activated by other divalent cations is consistent with this hypothesis. The dissociation constant of $Mn^{2+}{}_A$ in H101N arginase is measured by EPR spectroscopy to be 8 μM (data not shown), in good agreement with the activator constant of 7.6 μM for Mn^{2+} as determined in kinetic experiments in which activity was determined as a function of added Mn^{2+} (Figure 9). Furthermore, as discussed in the previous paragraph, assays run in the presence of 100 μM $MnCl_2$ reveal that metal-depleted H101N arginase can be nearly fully activated by excess Mn^{2+}. When metal-depleted H101N arginase is assayed in the presence of 1 mM concentrations of other divalent cations, significant activation by Co^{2+} and Cd^{2+} is observed; suprisingly, Zn^{2+} is inhibitory (data not shown). High-resolution X-ray crystal structure determinations of mixed-metal hybrid H101N arginases are obviously required to probe these novel structure−activity relationships, but differences in activation behavior may result from differences in metal coordination geometry and differences in the polarization of metal-bound solvent.

Engineering of Protein−Metal Binding Sites. It is informative to view the results with H101N arginase in view of histidine→asparagine metal ligand substitutions in the active sites of other metalloenzymes. More often than not, asparagine is *not* a satisfactory substitute for a histidine metal ligand. For example, H271 of *E. coli* D-xylose isomerase coordinates to a catalytically required Mn^{2+} or Mg^{2+} ion; the H271N variant exhibits catalytic activity that is 0.01% of that measured for the wild-type D-xylose isomerase, and the thermostability is decreased (Batt et al., 1990). No structure is reported for this enzyme variant, so the molecular basis for compromised function and stability cannot be determined. In the related D-xylose isomerase from *Streptomyces rubiginosus*, H220 coordinates to one of the manganese ions in a binuclear cluster; the crystal structure of the H220N variant reveals a fully-occupied binuclear manganese cluster, but N220 does not coordinate to manganese (Batt et al., 1990). The activity of H220N D-xylose isomerase is 0.3−0.5% of that measured for the wild-type D-xylose isomerase, and the T_m of the variant decreases 5−8 °C (Cha et al., 1994).

In this metalloenzyme, too, metal ligands have evolved with optimal chemical nature and conformation; structural perturbation of histidine→metal interactions compromises the structure, function, and stability of the binuclear metal cluster.

In alkaline phosphatase, H412 is a direct ligand to one of the two catalytic critically active site zinc atoms. The kinetic parameters of H412N alkaline phosphatase exhibit a strong zinc dependence. The metal-loaded H412N has 58% activity of wild-type alkaline phosphatase, while the metal-depleted H412N has 23% of wild-type activity (Ma & Kantrowitz, 1994). The structures of metal-loaded H412N and metal-depleted H412N alkaline phosphatase indicate that the Asn residue substituted for H412 does not coordinate to $Zn^{2+}{}_A$ (Ma et al., 1995).

The sole examples to date where histidine→asparagine substitutions yield viable transition metal ligands are in the active sites of H94N and H119N carbonic anhydrases II (Lesburg et al., 1997). In H119N carbonic anhydrase II, the side chain carbonyl of N119 coordinates to the active site zinc ion, and an additional solvent molecule joins the metal coordination polyhedron so that the coordination geometry changes from tetrahedral (as found in the wild-type enzyme) to trigonal bipyramidal. In H94N carbonic anhydrase II, the side chain carbonyl of N94 coordinates to zinc, and the side chain NH_2 donates a hydrogen bond to a zinc-bound Tris molecule; zinc coordination geometry is trigonal bipyramidal. These results suggest that a successful histidine→asparagine metal ligand substitution requires a certain degree of plasticity in the metal coordination polyhedron to accommodate structural changes resulting from the metal ligand substitution. Apparently, this degree of plasticity is unavailable in H220N xylose isomerase, H412N alkaline phosphatase, or H101N arginase. Despite the potentially isosteric nature of the histidine Nδ and asparagine Oδ atoms as metal ligands, asparagine does not appear to be an optimal substitution for a histidine ligand in a metalloprotein.

SUMMARY AND CONCLUSIONS

The X-ray crystal structures of metal-depleted native arginase, metal-loaded H101N arginase, and metal-depleted H101N arginase show that the substitution of a wild-type histidine ligand to Mn^{2+}_A compromises metal binding, which in turn compromises protein thermostability and catalytic function. The preparation of mixed-metal hybrid clusters with Mn^{2+} and Co^{2+} or Cd^{2+} restores some, but not all, catalytic function to metal-depleted H101N arginase; the preparation of a $Zn^{2+}-Mn^{2+}$ cluster is inhibitory. Clearly, an intact binuclear manganese cluster and ligand field are required for optimal catalysis and thermostability. It seems that the intact binuclear manganese cluster is necessary to maintain the catalytic nucleophile, metal-bridging hydroxide ion, in the proper location with the proper reactivity for optimal catalysis. Since no pH-dependent changes are observed in the tertiary or quaternary structure of the enzyme as the pH is raised from 8.5 to 9.0 (the optimum of catalytic activity), we conclude that increased arginase activity at higher pH values results from elevated concentrations of metal-bound hydroxide.

ACKNOWLEDGMENT

We thank Paul Lee for technical assistance with the measurement of CD spectra.

REFERENCES

Batt, C. A., Jamieson, A. C., & Vandeyar, M. A. (1990) *Proc. Natl. Acad. Sci. U.S.A. 87*, 618−622.

Bernstein, F. C., Koetzle, T. F., Williams, G. J. B., Meyer, E. F., Brice, M. D., Rodgers, J. R., Kennard, O., Shimanouchi, T., & Tasumi, M. (1977) *J. Mol. Biol. 112*, 535−542.

Boutard, V., Havouis, R., Fouqueray, B., Philippe, C., Moulinoux, J.-P., & Baud, L. (1995) *J. Immunol. 155*, 2077−2084.

Brünger, A. T., Kuriyan, J., & Karplus, M. (1987) *Science 235*, 458−460.

Cavalli, R. C., Burke, C. J., Kawamoto, S., Soprano, D. R., & Ash, D. E. (1994) *Biochemistry 33*, 10652−10657.

Cha, J., Cho, Y., Whitaker, R. D., Carrell, H. L., Glusker, J. P., Karplus, P. A., & Batt, C. A. (1994) *J. Biol. Chem. 269*, 2687−2694.

Christianson, D. W., & Alexander, R. S. (1989) *J. Am. Chem. Soc. 111*, 6412−6419.

Collaborative Computational Project, Number 4. (1994) *Acta Crystallogr. D50*, 760−763.

Corraliza, I. M., Soler, G., Eichman, K., & Modolell, M. (1995) *Biochem. Biophys. Res. Commun. 206*, 667−673.

Currie, G. A. (1978) *Nature 273*, 758−759.

Daghigh, F., Fukuto, J. M., & Ash, D. E. (1994) *Biochem. Biophys. Res. Commun. 202*, 174−180.

Herzfeld, A., & Raper, S. M. (1976) *Biochem. J. 153*, 469−478.

Hirsch-Kolb, H., Kolb, H. J., & Greenberg, D. M. (1971) *J. Biol. Chem. 246*, 395−401.

Kabsch, W. (1993) *J. Appl. Crystallogr. 26*, 795−800.

Kanyo, Z. F., Chen, C. Y., Daghigh, F., Ash, D. E., & Christianson, D. W. (1992) *J. Mol. Biol. 224*, 1175−1177.

Kanyo, Z. F., Scolnick, L. R., Ash, D. E., & Christianson, D. W. (1996) *Nature 383*, 554−557.

Kedra-Luboinska, M., Zamecka, E., & Porembska, Z. (1988) *Biochem. Med. Metab. Biol*., 247−257.

Kiefer, L. L., Paterno, S. A., & Fierke, C. A. (1995) *J. Am. Chem. Soc. 117*, 6831−6837.

Lesburg, C. A., & Christianson, D. W. (1995) *J. Am. Chem. Soc. 117*, 6838−6844.

Lesburg, C. A., Huang, C. C., Christianson, D. W., & Fierke, C. A. (1997) *Biochemistry* (submitted for publication).

Ma, L., & Kantrowitz, E. R. (1994) *J. Biol. Chem. 269*, 31614−31619.

Ma, L., Tibbitts, T. T., & Kantrowitz, E. R. (1995) *Protein Sci. 4*, 1498−1506.

Modolell, M., Corraliza, I. M., Link, F., Soler, G., & Eichmann, K. (1995) *Eur. J. Immunol. 25*, 1101−1104.

Morris, S. M., Bhamidipati, D., & Kepka-Lenhart, D. (1997) *Gene 193*, 157−161.

Navaza, J. (1994) *Acta Crystallogr. A50*, 157−163.

Nyborg, J., & Wonacott, A. J. (1977) in *The Rotation Method in Crystallogaphy* (Arndt, U. W., & Wonacott, A. J., Eds.) pp 139−152, North-Holland, Amsterdam.

Read, R. J. (1986) *Acta Crystallogr. A42*, 140−149.

Roholt, O. A., & Greenberg, D. M. (1956) *Arch. Biochem. Biophys. 62*, 454−470.

Sack, J. S. (1988) *J. Mol. Graphics 6*, 224−225.

Schueler, O., & Margalit, H. (1995) *J. Mol. Biol. 220*, 779−788.

Scolnick, L. R. (1997) Ph.D. Dissertation, University of Pennsylvania.

Southan, G. J., & Szabo, C. (1996) *Biochem. Pharmacol. 51*, 383−394.

Stuehr, D. J., Kwon, N. S., Nathan, C. F., Griffith, O. W., Feldman, P. L., & Wiseman, J. (1991) *J. Biol. Chem. 266*, 6259−6263.

Tabor, C. W., & Tabor, H. (1984) *Annu. Rev. Biochem. 53*, 749−790.

Wang, W. W., Jenkinson, C. P., Griscavage, J. M., Kern, R. M., Arabolos, N. S., Byrns, R. E., Cederbaum, S. D., & Ignarro, L. J. (1995) *Biochem. Biophys. Res. Commun. 210*, 1009−1016.

Weiner, C. P., Knowles, R. G., Stegink, L. D., Dawson, J., & Moncada, S. (1996) *Am. J. Obstet. Gynecol. 174*, 779−782.

Yip, M. C. M., & Knox, W. E. (1972) *Biochem. J. 127*, 839−899.

BI970800V